Stability of the regional stress field in central Japan during the late Quaternary inferred from the stress inversion of the active fault data

AUTHOR(S):

Tsutsumi, Hiroyuki; Sato, Katsushi; Yamaji, Atsushi

CITATION:

Tsutsumi, Hiroyuki ...[et al]. Stability of the regional stress field in central Japan during the late Quaternary inferred from the stress inversion of the active fault data. Geophysical Research Letters 2012, 39(23): L23303.

ISSUE DATE:

2012-12

URL:

http://hdl.handle.net/2433/167965

Stability of the regional stress field in central Japan during the late Quaternary inferred from the stress inversion of the active fault data

Hiroyuki Tsutsumi[1], Katsushi Sato[1], and Atsushi Yamaji[1]

[1]Division of Earth and Planetary Science, Graduate School of Science, Kyoto University, Kyoto 606-8502, Japan

ABSTRACT

We analyzed 169 geological fault-slip data from 37 active faults in central Japan to investigate the late Quaternary stress field stability. Modern stress states have been documented with unprecedented accuracy; however, their stability over time scales beyond instrumental observations is inadequately understood. Because the stress field has changed in the geological past, we compared present stress conditions in central Japan, determined from geophysical observations, with conditions determined by inverting the fault-slip data from active faults that exhibited cumulative displacement for the past ~10^5 years. The maximum stress axis obtained from fault-slip data trends ESE–WNW. This state of stress accounts for 97% of the data and supports the fact that oblique faults with reverse and strike-slip senses are interlaced in the region. The optimal stress is similar to the present stress state, indicating that the stress field in central Japan has been uniform and stable over the past ~10^5 years.

1. Introduction

The crustal stress field is one of the most important parameters required to understand tectonics, but the secular variation or stability of tectonic stress is not adequately understood for the time scales of 10^3–10^5 years. The World Stress Map (WSM) Project was the first coordinated effort to map tectonic stress fields worldwide [*Zoback*, 1992], and the WSM database released in 2008 [*Heidbach et al., 2010*] contains three times as much stress data as that of the 1992 database. Most of the data sets used to derive the stress fields in the project are geophysical data such as those derived from the focal-mechanism solutions of earthquakes and wellbore breakout. In contrast, geological data such as fault-slip data and volcanic-vent alignment accounted

for only ~10% of the total data [*Zoback*, 1992; *Heidbach et al.*, 2010]. The geophysical data reveal stress fields on the time scales of 10^0–10^2 years, whereas the geological data reveal stress fields over longer periods, usually 10^5 years or longer. Active faults are the clues that will help in filling the gap between the time scales of geophysical and geological observations because their intermittent but steadily growing displacements over the last 10^3–10^5 years are evident from, e.g., geomorphology, paleoseismic trenching, and seismic-reflection profiling. Central Japan is suitable for crustal stress-field analyses on different time scales because it contains one of the world's highest-quality geophysical [e.g., *Mazzotti et al.*, 2001; *Townend and Zoback*, 2006; *Terakawa and Matsu'ura*, 2010] and geological [e.g., *The Research Group for Active Faults of Japan*, 1991; *Nakata and Imaizumi*, 2002] data sets.

Permanent regional strain in central Japan has been accommodated mainly by active faults, which form a dense network in the region [*The Research Group for Active Faults of Japan*, 1991; *Nakata and Imaizumi*, 2002] (Figure 1). Since the 1995 Kobe earthquake, most of the long and fast-slipping faults in the region have been studied extensively through a national active-fault research program, which has produced one of the most comprehensive active-fault data sets in the world. Therefore, non-Andersonian faults have gradually become clear; reverse and strike-slip faults are interlaced in this region. In addition, a few of these types of faults have trends subparallel to each other while exhibiting different dip angles: the Hanaore and Biwako-seigan faults represent such a pair and are interpreted as an example of strain partitioning (Figure 1). Active faulting and its relation to the stress field in central Japan have been a topic of debate [*Huzita*, 1968; *Okada and Ando*, 1979], but the coexistence of faults with different senses of motion makes inference difficult without the inclusion of a special type of

55 stress-tensor inversion, as described below.

56 Stress-tensor inversion is used to determine stress conditions from the fault-slip data.
57 Each datum comprises the attitude of a fault and the slip direction on the fault plane
58 [e.g., *Angelier*, 1979] (Figure 2a). However, the slip directions are seldom determined
59 along the segments of active faults. Instead, the directions are vaguely documented in
60 the terms of slip senses. For example, the slip direction of a reverse fault has an
61 uncertainty of 180° with respect to the rake direction; the dip occurs at the center of
62 possible slip directions for the footwall block (Figure 2b). Similarly, the slip direction of
63 a strike-slip fault has an uncertainty of 180°, but the possible slip direction is horizontal
64 from the center of the slip. A few active faults in central Japan are described as oblique
65 reverse faults with sinistral or dextral components. The slip directions of these faults
66 have an uncertainty of 90° (Figure 2c). A fault-slip data set for active faults in central
67 Japan includes such deficiencies. *Lisle et al.* [2001] developed a pioneering
68 stress-inversion method to deal with sense-only data. Recently, *Sato* [2006] developed a
69 special type of stress-inversion method to deal with mixed set of complete and
70 sense-only fault-slip data.

71 In this study, we apply *Sato's* [2006] method to the active fault data to derive the
72 regional stress field in central Japan. Although the slip inversion of a single active fault
73 was conducted by *Blenkinsop* [2006] for the Chelungpu fault that ruptured during the
74 1999 Chi-Chi earthquake in Taiwan, this is the first study to reveal a regional stress field
75 based on the stress inversion analysis of a large set of the active fault data. We show that
76 central Japan is under an ESE–WNW compressional stress field with a small stress ratio,
77 $\Phi = (\sigma_2 - \sigma_3) / (\sigma_1 - \sigma_3)$, and that the regional stress field has been uniform and stable
78 over the past ~10^5 years.

2. Tectonic setting

To the east of the Japanese islands, the Pacific plate is subducted westward beneath the North American and Philippine Sea plates (Figure 1). Along the Nankai trough, the Philippine Sea plate has been subducting northwestward since the Pliocene or mid-Pleistocene [e.g., *Seno and Maruyama*, 1984; *Yamaji*, 2000]. In the study area, i.e., the eastern part of the southwest Japan arc, north-trending reverse faults and northwest-trending left-lateral and northeast-trending right-lateral strike-slip faults are densely distributed (Figure 1). The offsets of dated geomorphic features indicate slip rates in the order of 10^{-1} to 10^{0} mm/yr for such faults [*The Research Group for Active Faults of Japan*, 1991]. Central Japan has a long historical earthquake record that has been systematically collected for several centuries [*Usami*, 2003; *Ishibashi*, 2004]. The area has experienced one reverse-slip and four strike-slip earthquakes that ruptured the surface since the 1891 Nobi earthquake (Figure 1).

Geodetic and seismological data show that the Japan arc is subject to an approximate E–W compression. *Mazzotti et al.* [2001] calculated the permanent deformation field in central Japan by subtracting short-term elastic deformation related to the locking of the plate interface along the Nankai trough from GPS observations, and they obtained the residual-deformation field indicating ESE–WNW shortening. *Townend and Zoback* [2006] reported that the maximum horizontal stress is oriented approximately toward ENE–WSW in southwest Japan. *Terakawa and Matsu'ura* [2010] used the centroid-moment-tensor data to show that the tectonic stress of the Japan arc is basically an E–W compression with the direction of intermediate principal stress changing from N–S in northeast Japan to vertical in southwest Japan.

103

104 **3. Data**

105 After the 1995 Kobe earthquake, the Headquarters for Earthquake Research
106 Promotion (HERP) of the Japanese government selected approximately 100 inland
107 active faults and conducted extensive geological and paleoseismological studies to
108 assess their seismic potential. We compiled the fault-slip data from 36 active faults
109 selected by HERP in the Chubu and Kinki districts, to the west of the
110 Itoigawa–Shizuoka tectonic line and east of the Nojima fault that ruptured during the
111 1995 Kobe earthquake (Figure 1). To exclude local-stress perturbation due to the
112 collision of the Izu Peninsula with the main island of Japan [e.g., *Mazzotti et al.*, 2001;
113 *Townend and Zoback*, 2006] from our regional stress analysis, we analyzed the data for
114 the faults to the west of the Itoigawa–Shizuoka tectonic line, which is part of the
115 postulated plate boundary between the North American and Eurasian plates [*Nakamura*,
116 1983]. We examined data from paleoseismic trench walls, natural outcrops, and seismic
117 reflection profiles in published reports and maps. To determine the stress regime for a
118 time scale of 10^5 years, we compiled the data on faults that clearly offset geomorphic
119 surfaces or strata of late Quaternary age dated by tephrochronology or radiometric
120 methods. Therefore, we catalogued reliable fault orientations and slip senses at 166 sites
121 along 36 faults (Table S1 in the auxiliary material). In addition, we catalogued the data
122 from three sites along the Fukozu fault, the source fault of the 1945 Mikawa earthquake
123 that was not selected by HERP but for which extensive paleoseismic trenching was
124 conducted [e.g., *Sone and Ueta*, 1993].

125 The fault-slip data set used in this study had a few deficiencies. Slickenlines were
126 observed to determine the rakes of slip vectors at only 11 sites out of 169. We obtained

the “complete” data for 11 sites, and the remaining sites produced “sense-only” data, which have the rake uncertainties of 90° or 180° (Figures 2b and c). Figures 2d–f illustrate the tangent-lineation diagrams [*Twiss and Gefell*, 1990], improved by *Sato* [2006], that display the fault attitude and possible slip directions of the complete and sense-only data. A complete datum is denoted by an arrow plotted by a lower-hemisphere, equal-area projection; the pole of the fault plane is depicted in the stereogram by the position of the arrow, which itself indicates the slip direction of the footwall block (Figure 2d). The inward and outward directions of the arrow indicate the reverse and normal senses of shear, respectively. Strike-slip faults are represented by such arrows that are directed perpendicular to the radial directions in the plot. A sense-only datum is denoted by a semicircle or fan, which indicates the possible slip direction of the footwall block (Figures 2e and f). Figure 3 shows the fault-slip data from the active faults in the study area; we recorded a large variation of fault attitudes from 169 sites distributed along 37 faults.

4. Stress inversion

The stress-inversion method proposed by *Sato* [2006] was employed to determine the stress conditions that explain the mixed set of the complete and sense-only data. The method can deal with both the complete and sense-only data by placing tighter and looser constraints on the conditions, respectively. The Wallace–Bott hypothesis is assumed, as is customary: the slip directions of faults are assumed to be parallel to the resolved shear stresses (theoretical slip directions) on the fault planes, which are calculated from the fault attitudes and stress conditions. The fitness of arbitrary stress conditions to a datum, i.e., how preferable is the assumption for a fault, is defined as a

151 decreasing function of the misfit angle *d* between the theoretical and observed slip
152 directions (Figure 2g). The threshold in the function d_T is set to 30° in this study. For the
153 sense-only data, the misfit angles are measured from the center of possible slip
154 directions, and the degrees of fit are equal within the possible range (Figures 2h and i).
155 According to *Sato* [2006], all the types of fitness functions are normalized as
156 probability-density functions in the parameter space of deviatoric stress, which is
157 represented schematically as the heights of fitness values in Figures 2g–i. The degrees
158 of fit are added over the entire set of the complete and sense-only data to provide a total
159 fitness of stress conditions. The optimal stress conditions are searched to maximize the
160 total fitness. Although the complete data are uncommon in our database (Figure 3 and
161 Table S1), the large variation of fault orientations and large number of data enable us to
162 obtain a stress state with a relatively high precision.

163 Figure 4 shows the optimal stress for our data. A reverse-faulting stress-regime with
164 an ESE–WNW-trending σ_1-axis was found to be capable of explaining almost all the
165 data. The stress ratio, $\Phi = (\sigma_2 - \sigma_3) / (\sigma_1 - \sigma_3)$, was determined to be 0.09, which means
166 that the magnitude of σ_2 is approximately equal to that of σ_3. In addition, Figure 4
167 illustrates the uncertainty of the solution by plotting principal stress axes that have
168 fitness values greater than 90% of those of the optimal solution. Because of the small Φ
169 value (axial compressional stress), the σ_3-axis has a greater uncertainty than that of the
170 σ_1-axis. We calculated theoretical slip directions for the faults by assuming optimal
171 stress; white arrows in Figure 5 denote these directions.
172
173 **5. Discussion**

Despite the large variation of fault orientations (Figures 1 and 3), stress inversion revealed that almost all the active faults in the study area are consistent with a reverse-faulting stress regime with ESE–WNW-trending σ_1-axis (Figure 5). The theoretical slip directions of the faults calculated with this optimal stress were consistent with all the data except for five of them. Some of these exceptions have fault planes nearly perpendicular to the optimal σ_1-axis. Theoretical slip directions on such fault planes are unstable as is shown by the radial pattern around the σ_1-axis in Figure 5. Therefore, small perturbations in fault attitudes can explain the large misfits.

The optimal stress ratio of 0.09 indicates that σ_2 and σ_3 have similar values. Such a state of stress allows the coexistence of reverse and strike-slip faults, provided that they have different fault orientations. Their coexistence puzzled previous researchers who inferred the stress field from active faults in Japan because they assumed Andersonian faulting [*Huzita*, 1968; *Okada and Ando*, 1979]. Consequently, they neglected the coexistence of reverse and strike-slip faults or they had to infer spatially or temporarily complicated stress fields.

Although the ESE–WNW compression determined from active faults in this study is generally the same as that proposed by *Huzita* [1968], we demonstrated that a single state of stress explains the fault-slip data from all sites except five of them. This means that the stress field in central Japan has been uniform and that the active faults have slipped in the same directions over the past ~10^5 years. From the coexistence of reverse and strike-slip faults, we predicted that non-Andersonian, oblique-slip faulting is common in this region although the rakes of slip vectors were observed for only 10 of 37 faults.

The reactivation of the pre-existing planes of weakness gives rise to the

198 non-Andersonian faulting of planes with a wide variety of orientations. *Kano* [2002]
199 suggested that a few active faults are present in such planes in the Mesozoic
200 accretionary complex in the northern part of the study area. For example, the left-lateral
201 Yanagase fault (Figure 1) reactivated a kink plane of a map-scale chevron fold.
202 Similarly, the right-lateral Hanaore fault (Figure 1) lies along the axial surface of a fold
203 structure [*Kano*, 2002]. *Ito* [2006] obtained the apatite fission track ages of ~20 Ma for
204 dikes intruded along the Yanagase fault, which provides a minimum age constraint for
205 the fault. *Murakami and Tagami* [2004] conducted the zircon fission-track analysis of
206 pseudotachylyte sampled from the Nojima fault (Figure 1). They suggested that the
207 Nojima fault was already initiated at ~56 Ma. The active Median Tectonic Line (Figure
208 1) follows part of the boundary between the Ryoke and Sanbagawa terranes that were
209 accreted in the Mesozoic [*Hashimoto*, 1991]. Therefore, a few active faults in central
210 Japan reactivated the pre-existing faults under the present-day stress regime.
211 Slip on the active faults catalogued in this study reflects the average stress regime
212 in the late Quaternary. The inverted stress state determined in this study is principally
213 consistent with that obtained by geodetic and seismological data [*Mazzotti et al.*, 2001;
214 *Townend and Zoback*, 2006; *Terakawa and Matsu'ura*, 2010], suggesting that the stress
215 state in central Japan has been uniform and stable for the past ~10^5 years.
216
217 **6. Conclusions**
218 A dense distribution and an extensive data set of active faults in central Japan has
219 provided us with an exceptional opportunity to invert the regional stress field over a
220 time scale of ~10^5 years. We obtained an optimal state of stress, which is essentially the
221 same as that obtained by seismological and geodetic data, indicating that the stress field

222 in the eastern part of southwest Japan has been stable over the past ~10^5 years.
223 Moreover, the inversion results provide a clear explanation for the coexistence of
224 reverse and strike-slip faults in central Japan. Geological observations suggest that a
225 few active faults in central Japan reactivated pre-existing faults under the present-day
226 stress regime.
227
228 **Acknowledgments**
229 We thank Ritsuko Matsu'ura at the Association for the Development of Earthquake
230 Prediction for access to the literature on the active faults used in this study and Shigeru
231 Sueoka for his assistance in compiling the active fault database. We are grateful to
232 Richard Lisle and Robert Yeats for constructive reviews.
233
234 **References**
235 Angelier, J. (1979), Determination of the mean principal directions of stresses for a
236 given fault population, *Tectonophysics*, 56, T17-T26.
237 Blenkinsop, T. G. (2006), Kinematic and dynamic fault slip analyses: implications from
238 the surface rupture of the 1999 Chi-Chi, Taiwan, earthquake, *J. Struct. Geol.*, *28*,
239 1040-1050.
240 Hashimoto, M. (Ed.) (1991), *Geology of Japan*, Terra Scientific Publishing Company,
241 Tokyo.
242 Heidbach, O, M. Tingay, A. Barth, J. Reinecker, D. Kurfeß, and B. Müller (2010),
243 Global crustal stress pattern based on the World Stress Map database release 2008,
244 *Tectonophysics*, *428*, 3-15.
245 Huzita, K. (1968), Rokko movements and its appearance: intersecting structural patterns

of southwest Japan and Quaternary crustal movements, *Quaternary Res.*, *7*, 248-260. (in Japanese with English abstract)

Ishibashi, K. (2004), Status of historical seismology in Japan, *Ann. Geophys.*, *47*, 339-368.

Ito, H. (2006), Early Miocene igneous activity around northern part of the Yanagase fault and constraints on its fault activity from fission-track thermochronology, *J. Geol. Soc. Japan*, *112*, 612-615. (in Japanese with English abstract)

Kano, K. (2002), Steeply-plunging, map-scale folds in the Mino-Tanba Belt, Southwest Japan: origin of the Yanagase Fault as viewed from the basement structures, *J. Geol. Soc. Japan*, *108*, 591-605. (in Japanese with English abstract)

Kikuchi, M., and H. Kanamori (1996), Rupture process of the Kobe, Japan, earthquake of Jan. 17, 1995, determined from teleseismic body waves, *J. Phys. Earth*, *44*, 429-436.

Lisle, R., T. Orife, and L. Arlegui (2001), A stress inversion method requiring only slip sense, *J. Geophys. Res.*, *106*, 2281-2289.

Mazzotti, S., P. Henry, and X. Le Pichon (2001), Transient and permanent deformation of central Japan estimated by GPS: 2. Strain partition and arc-arc collision, *Earth Planet. Sci. Lett.*, *184*, 455-469.

Murakami, M., and T. Tagami (2004), Dating pseudotachylyte of the Nojima fault using the zircon fission-track method, *J. Geophys. Res.*, *31*, L12604, doi:10.1029/2004GL020211.

Nakamura, K. (1983), Possible nascent trench along the eastern Japan Sea as the convergent boundary between Eurasian and North American plates, *Bull. Earthq. Res. Inst. Univ. Tokyo*, *58*, 711-722. (in Japanese with English abstract)

Nakata, T., and T. Imaizumi (Eds.) (2002), *Digital Active Fault Map of Japan*, University of Tokyo Press, Tokyo. (in Japanese)

Okada, A., and M. Ando (1979), Active faults and earthquakes in Japan, *Kagaku*, *49*, 158-169. (in Japanese)

Sato, K. (2006), Incorporation of incomplete fault-slip data into stress tensor inversion, *Tectonophysics*, *421*, 319-330.

Seno, T., and S. Maruyama (1984), Paleogeographic reconstruction and origin of the Philippine Sea, *Tectonophysics*, *102*, 53-84.

Shiono, K. (1977), Focal mechanisms of major earthquakes in southwest Japan and their tectonic significance, *J. Phys. Earth*, *25*, 1-26.

Sone, K., and K. Ueta (1993), Trenching study of the Fukozu fault at Tokoji, Aichi Prefecture in 1988, *Active Fault Res.*, *11*, 43-46. (in Japanese)

Terakawa, T., and M. Matsu'ura (2010), The 3-D tectonic stress fields in and around Japan inverted from centroid moment tensor data of seismic events, *Tectonics*, *29*, TC6008, doi: 10.1029/2009TC002626.

The Research Group for Active Faults of Japan (Ed.) (1991), *Active Faults in Japan: Sheet Maps and Inventories (revised edition)*, University of Tokyo Press, Tokyo. (in Japanese with English abstract)

Townend, J., and M. D. Zoback (2006), Stress, strain, and mountain building in central Japan, *J. Geophys. Res.*, *111*, B03411, doi: 10.1029/2005JB003759.

Twiss, R. J., and M. J. Gefell (1990), Curved slickenfibers - a new brittle shear sense indicator with application to a sheared serpentinite, *J. Struct. Geol.*, *12*, 471-481.

Usami, T. (2003), *Materials for Comprehensive List of Destructive Earthquakes in Japan (latest edition)*, University of Tokyo Press, Tokyo. (in Japanese)

Yamaji, A. (2000), The multiple inverse method applied to meso-scale faults in mid-Quaternary fore-arc sediments near the triple junction off central Japan, *J. Struct. Geol.*, *22*, 429-440.

Zoback, M. L. (1992), First- and second-order patterns of stress in the lithosphere: the World Stress Map project, *J. Geophys. Res.*, *97*, 10703-11728.

Figure captions

Figure 1. Tectonic setting and distribution of active faults in the Kinki and Chubu districts of central Japan. The active fault traces (red lines) are from *Nakata and Imaizumi* [2002], and black arrows denote major strike-slip faults. Blue crosses denote the locations of outcrops, trench sites, and seismic-reflection profiles from where the fault-slip data were collected. Focal-mechanism solutions for historical surface-rupturing earthquakes are also shown by *Shiono* [1977] and *Kikuchi and Kanamori* [1996]: 1891 Nobi, 1927 Kita-Tango, 1945 Mikawa, 1948 Fukui, and 1995 Kobe earthquakes. Active faults mentioned in the text are Biwako-seigan fault: BF, Fukozu fault: FF, Hanaore fault: HF, Median Tectonic Line: MTL, Nojima fault: NF, and Yanagase fault: YF. Other abbreviations are Itoigawa–Shizuoka tectonic line: ISTL, Kyoto: Ky, Nagoya: Na, Osaka: O. Inset shows the plate-tectonic setting of Japanese islands. Eurasian plate: EU, Izu Peninsula: IP, North American plate: NA, Pacific plate: PA, Philippine Sea plate: PH. Thick arrows denote convergence directions between the Pacific and North American plates and between the Philippine Sea and Eurasian plates.

Figure 2. Types of fault-slip data and their constraints on stress condition. Figure (a)

shows a complete fault-slip datum comprising the attitude and slip direction of the fault. The direction is indicated by slickenlines on the fault plane. Figures (b) and (c) show the "sense-only" data obtained from faults on which slickenlines are not observed but whose sense of faulting is known from, for example, fault scarps and stream offsets. Either strike-slip sense or dip-slip sense of shear is known in (b), and both are known in (c). The possible slip directions of the footwalls are constrained within the range indicated by the semicircle and quadrant drawn on the fault plane. Figures (d–f) show the fault-slip data expressed in tangent-lineation diagrams [*Twiss and Gefell*, 1990] improved by *Sato* [2006]. Panels (d), (e), and (f) correspond to (a), (b), and (c), respectively. Figures (g–i) are graphs showing the fitness functions (bold lines) used in stress inversion, which can deal with all the types of the fault-slip data to determine the state of stress responsible for the observed fault movements. Figure (g) shows a fault with the complete data and the misfit angle d is between the theoretical and observed slip directions. Figures (h) and (i) show the case of a sense-only datum and d is defined as the angle formed by the theoretical slip direction and the central line of the semicircle or the fan.

Figure 3. Tangent-lineation diagram of the complete and sense-only fault-slip data obtained from the active faults in the study area. See Figure 2 for the explanations of the symbols.

Figure 4. Paired stereograms showing the range of stress conditions admissible for the fault-slip data in Figure 3. The stress ratios and principal orientations of the conditions are indicated by rainbow colors and lower-hemisphere, equal-area

342 projections. Stars denote the optimal orientations. The small circles are the
343 principal axes of stresses with fitness greater than 90% of that of the optimal
344 solution.
345
346 Figure 5. Optimal stress axes (open stars) and calculated theoretical slip directions
347 (white arrows) plotted on a tangent-lineation diagram with a lower-hemisphere,
348 equal-area projection. The fault-slip data are the same as that in Figure 3. The
349 fault-slip data shown in red are inconsistent with the theoretical slip directions.
350 Note that most of the data agree with the theoretical slip directions.

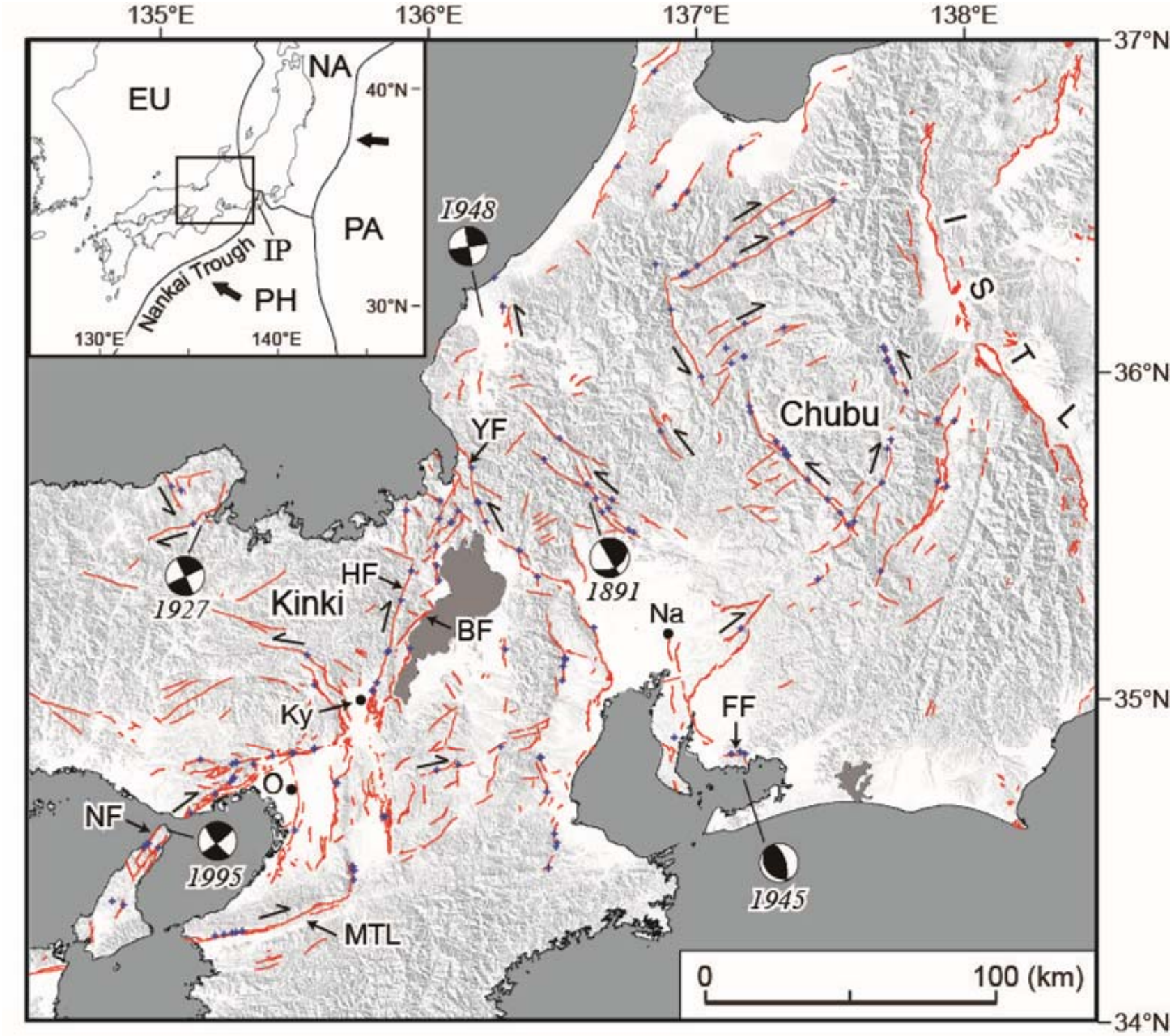
135°E
136°E
137°E
138°E
37°N
36°N
35°N
34°N
EU
NA
PA
PH
IP
Nankai Trough
40°N
30°N
130°E
140°E
1948
1927
1891
1945
1995
YF
HF
BF
MTL
NF
FF
Ky
O
Na
Kinki
Chubu
S
T
L
0
100 (km)

Figure 1.

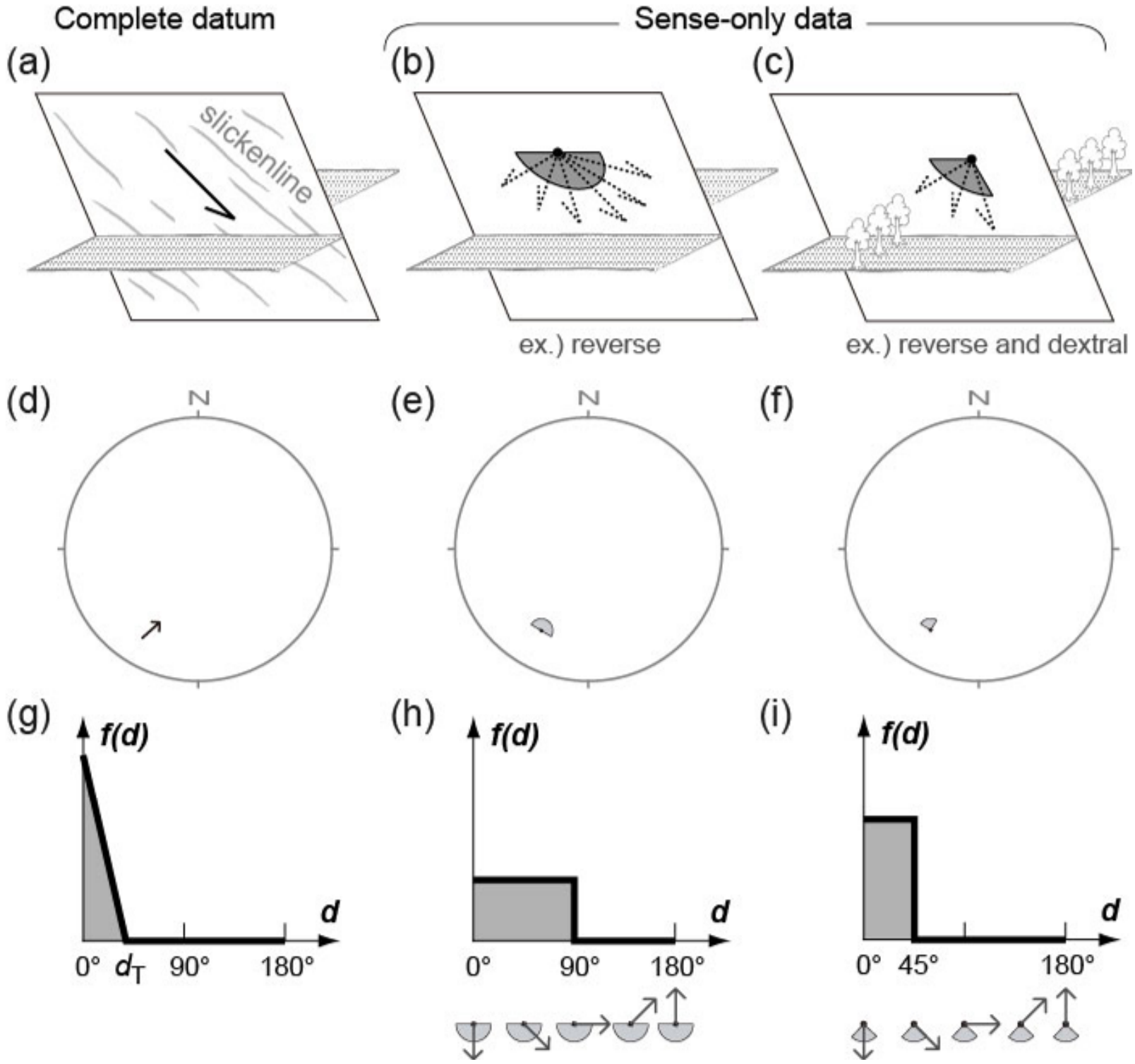
Complete datum
Sense-only data
(a)
(b)
(c)
slickenline
ex.) reverse
ex.) reverse and dextral
(d)
(e)
(f)
N
(g)
(h)
(i)
f(d)
d
0°
d_T
90°
180°
45°

Figure 2.

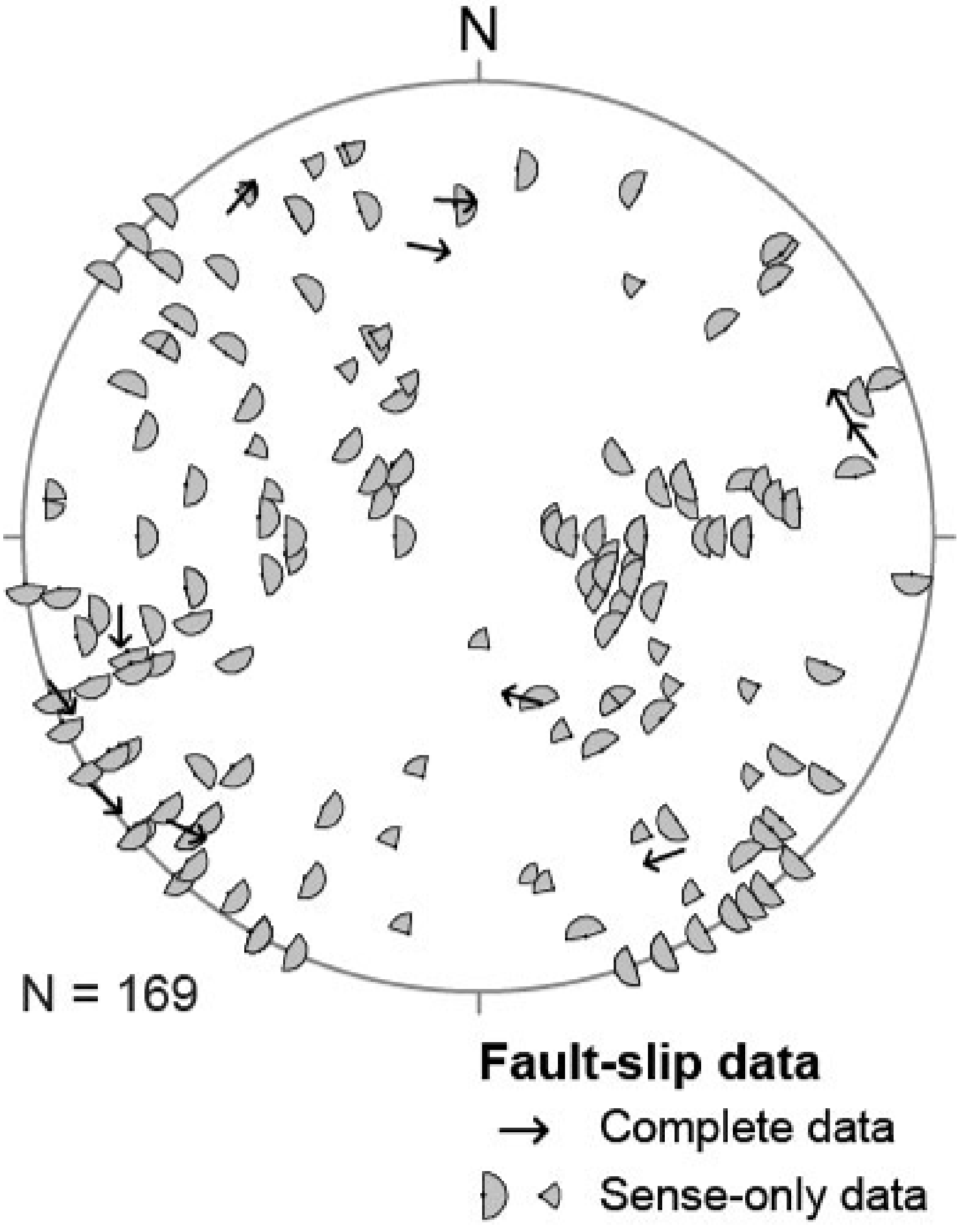

Figure 3.

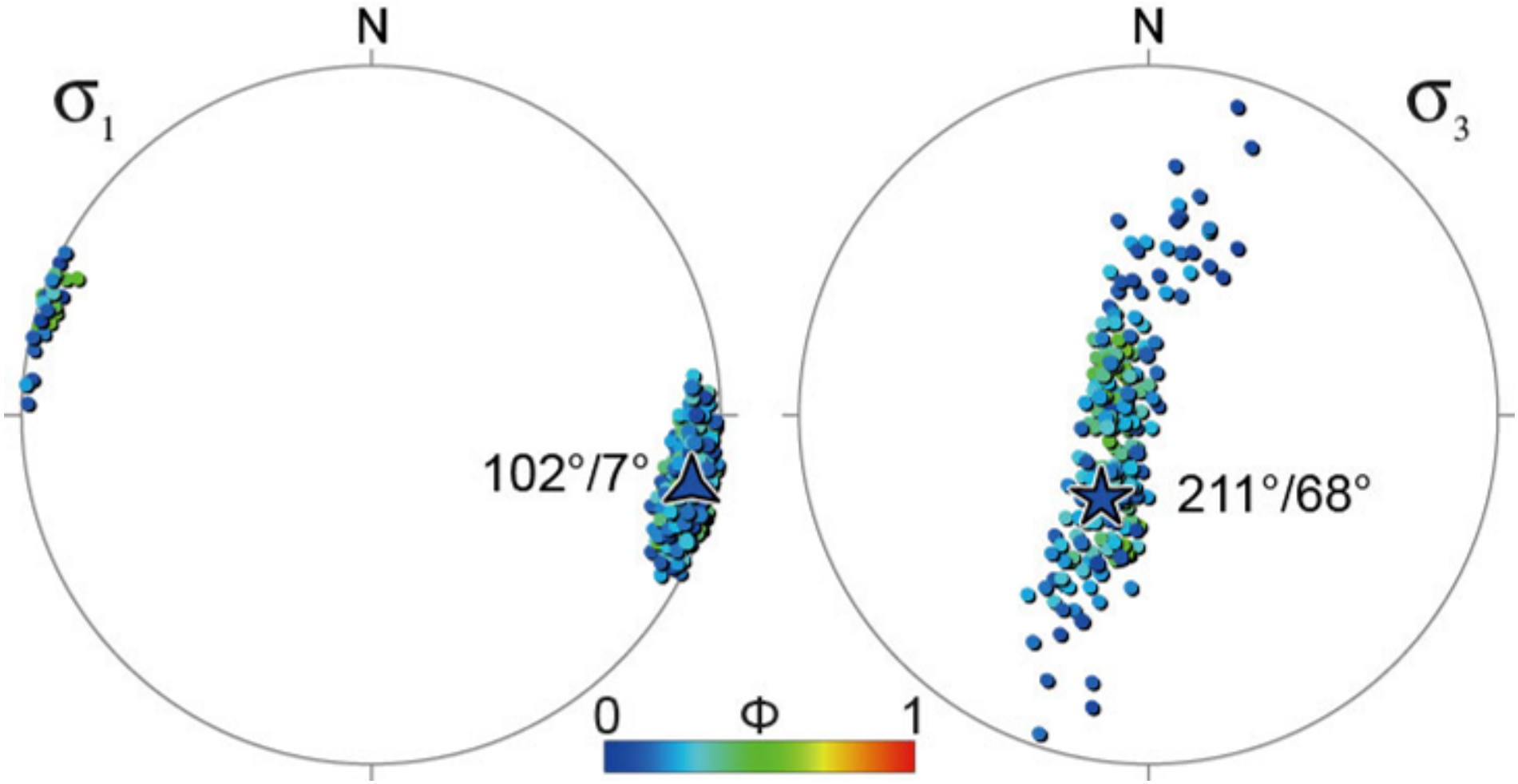

Figure 4.

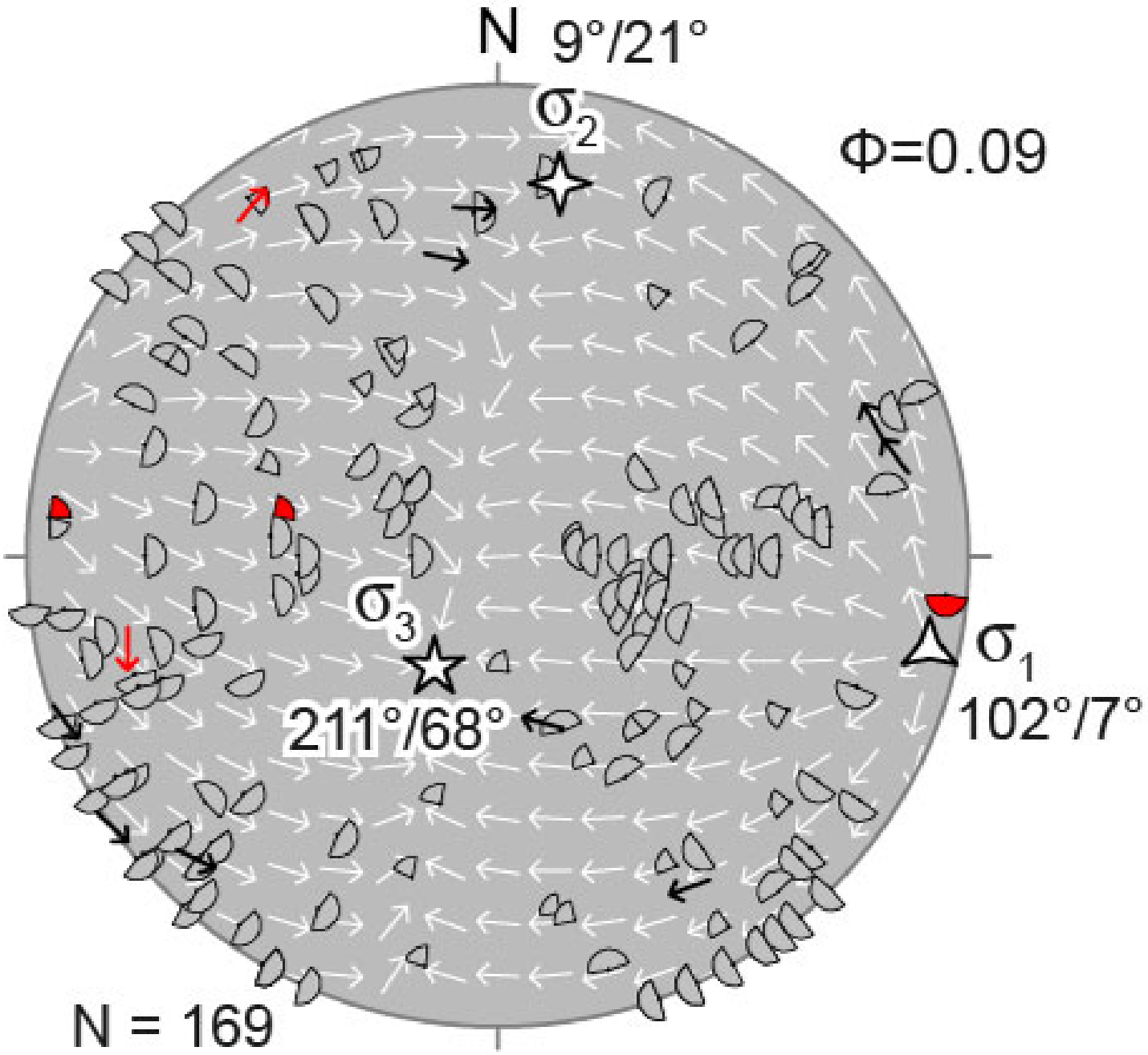

Fault-slip data with small misfit with large misfit

Complete data →

Sense-only data

→ Theoretical slip direction for optimal stress condition

Figure 5.

Table S1 Fault-slip data from 37 active faults in central Japan

Fault zone ID number1)	Name	Fault-slip data Site No.	Data source	Latitude (°N)	Longitude (°E)	Strike	Dip	Sense of slip	Rake of slip vector2)	Age of faulting3)	Inversion analysis Weight	Remarks	Dip direction4) Azimuth	Plunge	Slip orientation5) Azimuth	Plunge
45	Kisasamyakusein	45-1	natural outcrop	35.546	137.5859	NSE	85W	right-lateral		Holocene	1		275	85		
		45-2	natural outcrop	35.6054	137.6985	NS4E	55S	right-lateral		in the past 2000 years	1		144	55		
		45-3	trenching	35.7956	137.7247	N16E	30-50E	reverse, right-lateral		in the past 2000 years	1		100	40		
		45-4	trenching	35.768	137.7124	N25E	20E	reverse, right-lateral		Holocene	1		115	20		
46	Sakaitoge-Kamiya	46-1	trenching	35.9421	137.7811	N20W	65E (north wall)	left-lateral		in the past 2000 years	1		70	65		
		46-2	trenching	36.0672	137.783	N20W	80W-vertical	left-lateral		Holocene	1		250	85		
		46-3	trenching	36.0555	137.7999	N25W	70E-vertical	left-lateral		Holocene	1		70	80		
		46-4	trenching	35.9986	137.7348	N25W	40-60E	left-lateral		Holocene	1		65	50		
		46-5	natural outcrop	36.0779	137.6968	N12W	70E	left-lateral		late Pleistocene	0.5	close to 46-6	72	70		
		46-6	natural outcrop	36.0773	137.6963	N40W	58NE	left-lateral		late Pleistocene	0.5	close to 46-5	30	50		
		46-7	natural outcrop	36.0398	137.7115	N14W	70E	left-lateral	20N	Holocene	1		76	70	353.1	18.7
		46-8	natural outcrop	36.014	137.726	N40W	85E	left-lateral		Holocene	1		50	80		
47	Atotsugawa	47-1	trenching	36.3275	137.1376	N60E	65-75N	right-lateral	15W	historical (1858)	1		330	70	245.2	14.1
		47-2	natural outcrop	36.5218	137.5884	N55E	80SE	right-lateral	20-30W	historical (1858)	1		145	80	230.4	24.6
		47-3	geolicar survey	36.453	137.3181	N63E	vertical	right-lateral		historical (1858)	1		335	90		
		47-4	natural outcrop	36.4246	137.3511	N43E	88N	right-lateral		historical (1858)	1		313	80		
48	Takayama-Oppara	48-1	trenching	36.1479	137.1793	N60E	55-85S	right-lateral		Holocene	1		150	70		
		48-2	trenching	36.1372	137.3241	N70E	50-80S	right-lateral		Holocene	1		160	65		
		48-3	trenching	36.0466	137.1746	N45E	80NW-vertical	right-lateral		Holocene	0.5	close to 48-4	315	80		
		48-4	trenching	36.0483	137.1761	N35E	72NW	right-lateral		Holocene	0.5	close to 48-3	305	72		
		48-5	trenching	36.0278	137.1271	N58E	vertical	right-lateral		Holocene	1		328	90		
		48-6	natural outcrop	36.0749	137.1862	N35E	70SE	right-lateral		late Pleistocene	1		125	70		
49	Ushikubi	49-1	natural outcrop	36.2971	136.9433	N68E	70S	right-lateral		late Pleistocene	1		150	70		
		49-2	natural outcrop	36.3043	136.9613	N68E	40S	right-lateral		Holocene	1		150	40		
		49-3	trenching	36.3041	136.9592	N25E	vertical	right-lateral		in the past 2000 years	0.5	close to 49-4	325	90		
		49-4	trenching	36.3039	136.9586	N35E	vertical	right-lateral		in the past 2000 years	0.5	close to 49-3	325	90		
		49-5	trenching	36.3257	137.0086	N35E	60-70NW	right-lateral		in the past 2000 years	1		325	65		
		49-6	trenching	36.4073	137.1135	N45E	vertical	right-lateral		in the past 2000 years	1		315	90		
50	Shokawa	50-1	natural outcrop	36.3294	136.8429	N30W	vertical	left-lateral		late Pleistocene	1		60	90		
		50-2	trenching	36.1089	136.9819	N10W	40-60W	left-lateral		Holocene	1		260	50		
		50-3	trenching	35.9871	137.0146	N20W	70E	left-lateral		historical (1586)	1		70	70		
51	Inadani	51-1	seismic profiling	35.8161	137.0374	N20E	30-40W	reverse		late Pleistocene	1		290	35		
		51-2	seismic profiling	35.6521	137.9312	N25E	20-30W	reverse		late Pleistocene	1		295	25		
		51-3	trenching	35.6675	137.8959	NS	20-25W	reverse		Holocene	1		270	22.5		
		51-4	trenching	35.8521	137.9686	N30E	25-55W	reverse		late Pleistocene	1		320	40		
		51-5	trenching	35.3927	137.6865	N30E	40W	right-lateral, reverse		historical (1586 or 1718)	1		300	40		
52	Atera	52-1	natural outcrop	35.897	137.1945	N6W	vertical	left-lateral		late Pleistocene	1		84	90		
		52-2	natural outcrop	35.8881	137.1989	N23W	88E	left-lateral	25-34S	late Pleistocene	1		69	88	157.9	29.5
		52-3	natural outcrop	35.7483	137.5297	N63W	73NE	left-lateral		late Pleistocene	1		27	73		
		52-4	trenching	35.7897	137.2952	N45W	80NE	left-lateral		historical (1586)	0.5	close to 52-5	45	80		
		52-5	trenching	35.7891	137.2962	N45W	80NE	left-lateral		historical (1586)	0.5	close to 52-4	45	80		
		52-6	natural outcrop	35.7676	137.3227	N7W	82E	left-lateral		late Pleistocene	1		83	82		
		52-7	natural outcrop	35.7551	137.3319	N40W	88NE	left-lateral		in the past 2000 years	1		50	80		
		52-8	trenching	35.7456	137.3486	N45W	75NE	left-lateral		Holocene	1		45	75		
		52-9	trenching	35.6727	137.4137	N40W	vertical	left-lateral		Holocene	1		42	90		
		52-10	natural outcrop	35.6125	137.487	N30W	80NE	left-lateral		Holocene	1		60	80		
		52-11	trenching	35.5715	137.5368	N45W	75NE	left-lateral		Holocene	1		45	75		
		52-12	trenching	35.5356	137.5656	N42W	80SW	left-lateral		Holocene	0.5	close to 52-13	228	80		
		52-13	trenching	35.5347	137.5668	N40W	85NE	left-lateral		Holocene	0.5	close to 52-14	42	85		
53	Ryobuyama-Enasan	53-1	trenching	35.3689	137.4524	N50E	30-50SE	reverse, right-lateral		Holocene	1		140	40		
54	Sonogeyama	54-1	trenching, borehole survey	35.2173	137.1631	N40E	80SE	right-lateral		Holocene	1		130	80		
		54-2	seismic profiling	34.8815	136.9141	N20W	80W	reverse		late Pleistocene	1		250	80		
55	Ouchigata	55-1	seismic profiling	36.9126	136.8487	N40E	20SE	reverse		late Pleistocene	0.5	close to 55-2	130	20		
		55-2	trenching	36.9123	136.8484	N40E	20SE	reverse		in the past 2000 years	0.5	close to 55-1	130	20		
56	Tonamiheiya-Kurehayama	56-1	seismic profiling	36.5653	136.8541	N45E	45-50W	reverse		late Pleistocene	1		315	47.5		
		56-2	trenching	36.5478	136.9688	N30E	30S	reverse		Holocene	1		150	30		
		56-3	trenching	36.5865	136.9183	N20E	20E	reverse		Holocene	1		110	20		
		56-4	seismic profiling	36.6815	137.1617	N30E	45NW	reverse		late Pleistocene	1		330	45		
57	Morimoto-Togashi	57-1	trenching	36.6239	136.7829	N30E	23E	reverse		Holocene	1		120	23		
58	Fukuiheiyatoen	58-1	natural outcrop	36.2981	136.2397	N0-15W	62E-vertical	reverse		late Pleistocene	1		78.5	76		
		58-2	trenching	36.3398	136.2727	NSE	80E-vertical	left-lateral, reverse		Holocene	1		95	85		
59	Nagaragawajuryu	59-1	natural outcrop	35.8222	136.8629	N0-10W	65-80W	left-lateral		late Pleistocene	1		261	72.5		
60	Nobi	60-1	trenching	35.6589	136.5868	N40W	60SW	left-lateral		historical (1981)	1		230	60		
		60-2	trenching	35.512	136.7083	N60W	vertical	left-lateral		historical (1981)	1		30	90		
		60-3	trenching	35.5221	136.7413	N60W	vertical	left-lateral		historical (1981)	1		30	90		
		60-4	natural outcrop	35.5857	136.6678	N43W	63E	left-lateral		historical (1981)	1		47	63		
		60-5	trenching	35.5757	136.6433	N30W	83E	left-lateral		historical (1981)	1		60	83		
		60-6	trenching	35.7998	136.4858	N65W	70-75SW	left-lateral		historical (1981)	1		205	72.5		
		60-7	trenching	35.6159	136.6287	N35W	vertical	left-lateral	24S	historical (1981)	1		55	90	145	24
		60-8	trenching	35.7356	136.4225	N40W	vertical	left-lateral		in the past 2000 years	0.5	close to 60-9	50	90		
		60-9	trenching	35.7364	136.4264	N40W	60SW-vertical	left-lateral		in the past 2000 years	0.5	close to 60-8	230	75		
		60-10	natural outcrop	35.6124	136.6818	N55W	85NE	left-lateral		late Pleistocene	1		35	85		
61	Yanagase	61-1	natural outcrop	35.5438	136.289	N43W	80SW	left-lateral		late Pleistocene	1		227	80		
		61-2	natural outcrop	35.5811	136.1821	N24W	vertical	left-lateral		Holocene	1		66	90		
		61-4	trenching	35.6084	136.1768	N17-22W	67-80W	left-lateral	10-20N	historical (1325)	1		258.5	73.5	336.1	14.4
		61-6	natural outcrop	35.7093	136.1566	N10-20W	50-60E	left-lateral		late Pleistocene	1		75	55		
		61-7	trenching	35.4567	136.1344	N60W	vertical	left-lateral		Holocene	0.5	close to 61-8	30	90		
		61-8	trenching	35.4579	136.1325	N60W	vertical	left-lateral		Holocene	0.5	close to 61-7	30	90		
62	Sekigahara	62-1	natural outcrop	35.3759	136.481	N14W	80E	reverse		Holocene	1		76	80		
63	Nosaka-Shufukuji	63-1	trenching	35.0888	136.0376	N65W	vertical	left-lateral		historical (1662?)	1		25	90		
64	Kohokusanchi	64-1	pit excavation	35.5783	136.1852	N30E	70E	right-lateral		in the past 2000 years	1		120	70		
		64-2	pit excavation	35.5444	136.0887	N45E	70E	right-lateral		Holocene	0.5	close to 64-3	135	70		
		64-3	trenching, pit excavation	35.5426	136.0774	N50-55E	vertical	right-lateral		in the past 2000 years	0.5	close to 64-2	322.5	90		
		64-4	trenching	35.5538	136.0336	N28E	45E	right-lateral, reverse		historical (1325)	1		118	45		
65	Biwakoseigan	65-1-1	seismic profiling	35.1572	135.9244	N13W	40W (0-5km depth)	reverse		late Pleistocene	0.5	close to 65-1-2	255	40		
		65-1-2					35W (5-5km depth)	reverse			0.5	close to 65-1-1	255	35		
		65-2	trenching	35.4719	136.0246	N25E	30NW	reverse		Holocene	1		295	30		
		65-3	trenching	35.4389	136.0244	N20E	15-30W	reverse		Holocene	1		290	22.5		
		65-4-1	trenching	35.3658	136.0526	N10E	25W (No. 1 trench)	reverse		Holocene	0.333	close to 65-4-2, 3	280	25		
		65-4-2				N10E	30W (No. 2 trench)	reverse		Holocene	0.333	close to 65-4-3, 1	280	30		
		65-4-3				NS	50W (No. 3 trench)	reverse		Holocene	0.333	close to 65-4-1, 2	270	50		
67	Yoro-Kuwana-Yokkaichi	67-1	seismic profiling	35.2282	136.6153	N30W	30W	reverse		late Pleistocene	1		240	30		
68	Suzukatoen	68-1	seismic profiling	35.1261	136.5862	N5W	60W	reverse		late Pleistocene	1		265	60		
		68-2	natural outcrop	35.1288	136.5854	NS	30W	reverse		late Pleistocene	1		270	30		
		68-3	trenching	35.1268	136.5811	N5W	60W	reverse		in the past 2000 years	1		265	60		
		68-4	trenching	35.382	136.4973	N15E	30W	reverse		Holocene	1		285	30		
		68-5	trenching	35.0577	136.4953	N35E	30W	reverse		Holocene	1		305	30		
69	Suzukaseien	69-1	seismic profiling	35.1529	136.2885	N5W	30-40E	reverse			1		85	35		
70	Tongu	70-1	natural outcrop	34.8522	136.2646	NS	60-68E	reverse		late Pleistocene	1		90	64		
71	Nunobikisanchitoen	71-1	trenching	34.8187	136.4156	N10W	15W	reverse		late Pleistocene	0.5	close to 71-2	260	15		
		71-2	trenching	34.8171	136.4147	N10W	30-50W	reverse		late Pleistocene	0.5	close to 71-1	80	40		
		71-3	trenching	34.8179	136.411	N15W	65E	reverse		late Pleistocene	0.5	close to 71-4	75	65		
		71-4	seismic profiling	34.8193	136.4154	N10W	50-60W	reverse		late Pleistocene	0.5	close to 71-3	260	55		
		71-5	seismic profiling	34.713	136.438	NS	50W	reverse		late Pleistocene	1		270	50		
		71-6	natural outcrop	34.5553	136.4754	N10W	30-50W	reverse		late Pleistocene	1		260	40		
		71-7	trenching	34.5837	136.4649	N5W	15W	reverse		Holocene	1		265	15		
		71-8	natural outcrop	34.5421	136.4705	N5W	15W	reverse		Holocene	1		265	15		
		71-9	trenching	34.4785	136.4458	N15W	40W	reverse		late Pleistocene	1		255	40		
72	Kizugawa	72-1	trenching	34.7957	136.1842	N65E	30-50N	reverse, right-lateral		historical (1854)	1		335	40		
		72-2	trenching	34.7783	136.8242	N40E	60N	reverse, right-lateral		in the past 2000 years	1		350	60		
73	Mikata-Hanaore	73-1	trenching	35.5808	135.91	NSE	30-50E	reverse		in the past 2000 years	1		95	40		
		73-2	trenching	35.3955	135.9298	N34E	vertical	right-lateral		historical (1662)	0.5	close to 73-3	124	90		
		73-3	trenching	35.3932	135.929	N26E	60-80W	right-lateral		historical (1662)	0.5	close to 73-2	298	70		
		73-4	natural outcrop	35.3844	135.8917	N26E	58SE	right-lateral		late Pleistocene	1		126	58		
		73-5	natural outcrop	35.1493	135.8452	N28-25E	70-75E	right-lateral		late Pleistocene	1		112.5	72.5		
		73-6	natural outcrop	35.144	135.8415	N24E	82NW	right-lateral		late Pleistocene	1		304	82		
		73-7	trenching	35.0584	135.8089	N30E	60-80E	right-lateral, reverse		Holocene	1		120	70		
		73-8-1	trenching	35.0249	135.7862	N30-40E	30E	reverse		Holocene	0.333	close to 73-8-2, 73-9	125	30		
		73-8-2	borehole survey			N30E	50E	reverse		Holocene	0.333	close to 73-8-1, 73-9	120	50		
		73-9	borehole survey	35.0248	135.7839	N10E	50-60E	reverse		Holocene	0.333	close to 73-8-1, 73-8-2	100	55		
74	Yamada	74-1	trenching	35.5393	135.1116	N50E	40NW	right-lateral, reverse		historical (1927)	1		320	40		
		74-2	trenching	35.6413	135.0674	N20W	vertical	left-lateral		late Pleistocene	1		70	90		
		74-3	trenching	35.6525	135.0527	N14W	70SW	left-lateral, reverse	30-40N	historical (1927)	1		256	76	336.4	33.8
75	Kyotobanchi-Naradonchi	75-1	seismic profiling	34.6351	135.8226	N10W	50-60E	reverse		late Pleistocene	1		80	55		
		75-2	seismic profiling	34.635	135.8347	N10W	50-60E	reverse		late Pleistocene	1		80	55		
76	Arima-Takatsuki	76-1	natural outcrop	34.7977	135.2586	N62E	42S	right-lateral, reverse		historical (1596)	1		152	42		
		76-2	natural outcrop	34.8834	135.2733	N80E	63S	right-lateral, reverse	5-15E	Holocene	0.5	close to 76-3	176	63	98.6	8.9
		76-3	trenching	34.8856	135.2749	N63E	32S	right-lateral, reverse		historical (1596)	0.5	close to 76-2	153	32		
		76-4	trenching	34.825	135.4189	N40E	vertical	right-lateral		historical (1596)	1		330	90		
		76-5	trenching	34.8321	135.4421	N70E	vertical	right-lateral		historical (1596)	0.5	close to 76-6	340	90		
		76-6	natural outcrop	34.8329	135.4881	N70E	vertical	right-lateral		historical (1596)	0.5	close to 76-5	340	90		
		76-7	trenching	34.849	135.5677	N65E	vertical	right-lateral		historical (1596)	1		335	90		
		76-8	trenching	34.8427	135.5658	N70E	70S-vertical	right-lateral, reverse		historical (1596)	1		160	80		
77	Ikoma	77-1	seismic profiling	34.742	135.6471	NS	30-40E	reverse		late Pleistocene	0.5	close to 77-2	90	35		
		77-2	trenching	34.7579	135.6587	NS	15E	reverse		in the past 2000 years	0.5	close to 77-1	90	15		
78	Mitake-Kyotonishiyama	78-1	trenching	35.1361	135.539	N45W	80NE	left-lateral, reverse	28E	Holocene	1		45	80	129.7	27.5
		78-2	seismic profiling	35.0448	135.5679	N40W	70NE	reverse		late Pleistocene	1		50	70		
79	Rokko-Awajishima	79-1	borehole survey	34.7982	135.3394	NS	40-45W	reverse		late Pleistocene	1		270	42.5		
		79-2-1	trenching	34.8114	135.1393	N14W	70S (west wall)	right-lateral		late Pleistocene	0.5	close to 79-2-2	186	70		
		79-2-2				N40E	62S (east wall)			late Pleistocene	0.5	close to 79-2-1	176	62		
		79-3-1	trenching	34.6452	135.1046	N73E	68N (east wall)	right-lateral, reverse		historical (1596)	0.5	close to 79-3-2	348	68		
		79-3-2				N58E	82N (west wall)			historical (1596)	0.5	close to 79-3-1	328	82		
		79-4	trenching	34.3626	134.8517	N15E	20-30W	reverse		historical (1596)	1		285	25		
		79-5-1	natural outcrop	34.3746	134.8188	N58E	62W (eastern strand)	reverse		late Pleistocene	0.5	close to 79-5-2	328	82		
		79-5-2				N75E	80W (western strand)			late Pleistocene	0.5	close to 79-5-1	345	80		
		79-6	trenching	34.5384	134.9823	N40E	vertical	right-lateral		historical (1596)	1		130	90		
		79-7	trenching	34.554	134.9454	NSE	85E	right-lateral, reverse		historical (1995)	0.5	close to 79-8	95	85		
		79-8	trenching	34.5524	134.942	N71E	88S	right-lateral, reverse		historical (1995)	0.5	close to 79-7	161	88		
		79-9	trenching	34.5494	134.9371	N65E	88S	right-lateral, reverse		historical (1995)	1		155	88		
		79-10	trenching	34.5415	134.9269	N55E	82S	right-lateral, reverse		historical (1995)	1		145	82		
		79-11	natural outcrop	34.786	135.1947	N45E	vertical	right-lateral		late Pleistocene	1		135	90		
		79-12	natural outcrop	34.7422	135.2522	N40E	70W	right-lateral, reverse		historical (1596)	1		310	70		
		79-13	natural outcrop	34.7514	135.2616	N29-36E	46-72W	right-lateral, reverse		late Pleistocene	1		298	59		
		79-14	natural outcrop	34.7566	135.2654	N30E	40W	right-lateral, reverse		Holocene	1		306	46		
80	Uemachi	80-1	seismic profiling	34.5944	135.494	N10-25E	65-70E	reverse		late Pleistocene	1		107.5	67.5		
81	Median Tectonic Line (Ikumisanchi-Kongosanchitoen)	81-1	trenching	34.2711	135.2284	N75E	27-33N	right-lateral, reverse	30N	Holocene	1		345	30	281.6	14.5
		81-2	natural outcrop	34.2667	135.1955	N60E	65N	right-lateral, reverse		late Pleistocene	1		330	65		
		81-3	trenching	34.2814	135.2962	N75W	68N	right-lateral, reverse		late Pleistocene	1		15	68		
		81-4	trenching	34.2763	135.2579	N77W	45N	right-lateral, reverse		Holocene	0.5	close to 81-5	13	45		
		81-5	trenching	34.2763	135.2575	N80W	70-85N	right-lateral, reverse		Holocene	0.5	close to 81-4	10	77.5		
		81-6	trenching	34.2782	135.2729	N85E	30-38N	right-lateral, reverse		Holocene	1		355	28		
		81-7	natural outcrop	34.441	135.713	N70E	20-45N	reverse		in the past 2000 years	1		340	32.5		
		81-8	seismic profiling	34.462	135.7123	NS	30W	reverse		late Pleistocene	0.5	close to 81-9	270	30		
		81-9	seismic profiling	34.4814	135.7066	NS	45W	reverse		late Pleistocene	0.5	close to 81-8	270	45		
		81-10	seismic profiling	34.4698	135.7164	NS	30W	reverse		late Pleistocene	0.5	close to 81-11	270	30		
		81-11	seismic profiling	34.47	135.7115	NS	15-20W	reverse		late Pleistocene	0.5	close to 81-10	270	17.5		
n/a	Fukuzuru	Fu-1	trenching	34.8297	137.1788	N7W	53-61W	reverse		historical (1945)	1		263	57		
		Fu-2	trenching	34.8368	137.1594	N57W	56S	reverse, left-lateral		historical (1945)	1		213	56		
		Fu-3	trenching	34.8288	137.1274	N80E	54S	reverse, left-lateral	25E	historical (1945)	1		170	54	244.7	20

1) Designated by the Headquarters of Earthquake Research Promotion of the Japanese government (http://www.jishin.go.jp/main/index.html).
2) Rake angle of slip direction measured downward from the direction of strike identified by the last character.
3) Timing of the last faulting event or the age of faulted geomorphic surface or stratum.
4) Azimuth and plunge of the dip directions of the fault planes. When the strike or dip is shown within a range, the mean value was used for the inversion analysis.
5) Azimuth and plunge of the slip orientations without shear senses. When the rake is shown within a range, the mean value was used for the inversion analysis.
Fault-slip data from sites 45-1, 45-3, 46-7, 47-2, and 79-7 are inconsistent with the theoretical slip directions.